

High-Statistics Measurement of Antineutrino Quasielastic-like scattering at $E_\nu \sim 6$ GeV on a Hydrocarbon Target

A. Bashyal,^{1,*} S. Akhter,² Z. Ahmad Dar,^{3,2} F. Akbar,² V. Ansari,² M. V. Ascencio,^{4,†} M. Sajjad Athar,² A. Bercellie,⁵ M. Betancourt,⁶ A. Bodek,⁵ J. L. Bonilla,⁷ A. Bravar,⁸ H. Budd,⁵ G. Caceres,^{9,‡} M.F. Carneiro,^{1,9,§} G.A. Díaz,⁵ J. Felix,⁷ L. Fields,¹⁰ A. Filkins,³ R. Fine,^{5,¶} A.M. Gago,⁴ H. Gallagher,¹¹ P.K.Gaur,² S.M. Gilligan,¹ R. Gran,¹² E.Granados,⁷ D.A. Harris,^{13,6} S. Henry,⁵ S. Jena,¹⁴ J. Kleykamp,^{5,**} A. Klustová,¹⁵ M. Kordosky,³ D. Last,¹⁶ T. Le,^{11,17} A. Lozano,⁹ X.-G. Lu,^{18,19} E. Maher,²⁰ S. Manly,⁵ W.A. Mann,¹¹ C. Mauger,¹⁶ K.S. McFarland,⁵ A.M. McGowan,⁵ B. Messerly,^{21,††} J. Miller,²² O. Moreno,^{3,7} J.G. Morfin,⁶ D. Naples,²¹ J.K. Nelson,³ C. Nguyen,²³ V. Paolone,²¹ G.N. Perdue,^{6,5} K.-J. Plows,¹⁹ M.A. Ramírez,^{16,7} H. Ray,²³ D. Ruterbories,⁵ H. Schellman,¹ C.J. Solano Salinas,²⁴ H. Su,²¹ M. Sultana,⁵ V.S. Syrotenko,¹¹ E. Valencia,^{3,7} N.H. Vaughan,¹ A.V. Waldron,^{25,15} C. Wret,⁵ B. Yaeggy,^{22,‡‡} and L. Zazueta³

(The MINERvA Collaboration)

¹*Department of Physics, Oregon State University, Corvallis, Oregon 97331, USA*

²*Department of Physics, Aligarh Muslim University, Aligarh, Uttar Pradesh 202002, India*

³*Department of Physics, William & Mary, Williamsburg, Virginia 23187, USA*

⁴*Sección Física, Departamento de Ciencias, Pontificia Universidad Católica del Perú, Apartado 1761, Lima, Perú*

⁵*Department of Physics and Astronomy, University of Rochester, Rochester, New York 14627 USA*

⁶*Fermi National Accelerator Laboratory, Batavia, Illinois 60510, USA*

⁷*Campus León y Campus Guanajuato, Universidad de Guanajuato, Lascruain de Retana No. 5, Colonia Centro, Guanajuato 36000, Guanajuato México.*

⁸*University of Geneva, 1211 Geneva 4, Switzerland*

⁹*Centro Brasileiro de Pesquisas Físicas, Rua Dr. Xavier Sigaud 150, Urca, Rio de Janeiro, Rio de Janeiro, 22290-180, Brazil*

¹⁰*Department of Physics, University of Notre Dame, Notre Dame, Indiana 46556, USA*

¹¹*Physics Department, Tufts University, Medford, Massachusetts 02155, USA*

¹²*Department of Physics, University of Minnesota – Duluth, Duluth, Minnesota 55812, USA*

¹³*York University, Department of Physics and Astronomy, Toronto, Ontario, M3J 1P3 Canada*

¹⁴*Department of Physical Sciences, IISER Mohali, Knowledge City, SAS Nagar, Mohali - 140306, Punjab, India*

¹⁵*The Blackett Laboratory, Imperial College London, London SW7 2BW, United Kingdom*

¹⁶*Department of Physics and Astronomy, University of Pennsylvania, Philadelphia, PA 19104*

¹⁷*Rutgers, The State University of New Jersey, Piscataway, New Jersey 08854, USA*

¹⁸*Department of Physics, University of Warwick, Coventry, CV4 7AL, UK*

¹⁹*Oxford University, Department of Physics, Oxford, OX1 3PJ United Kingdom*

²⁰*Massachusetts College of Liberal Arts, 375 Church Street, North Adams, MA 01247*

²¹*Department of Physics and Astronomy, University of Pittsburgh, Pittsburgh, Pennsylvania 15260, USA*

²²*Departamento de Física, Universidad Técnica Federico Santa María, Avenida España 1680 Casilla 110-V, Valparaíso, Chile*

²³*University of Florida, Department of Physics, Gainesville, FL 32611*

²⁴*Facultad de Ciencias, Universidad Nacional de Ingeniería, Apartado 31139, Lima, Perú*

²⁵*G O Jones Building, Queen Mary University of London, 327 Mile End Road, London E1 4NS, UK*

(Dated: November 23, 2022)

We present measurements of the cross section for anti-neutrino charged-current quasielastic-like scattering on hydrocarbon using the medium energy (ME) NuMI wide-band neutrino beam peaking at $\langle E_\nu \rangle \sim 6$ GeV. The cross section measurements are presented as a function of the longitudinal momentum ($p_{||}$) and transverse momentum (p_T) of the final state muon. This work complements our previously reported high statistics measurement in the neutrino channel and extends the previous anti-neutrino measurement made in the low energy (LE) beam at neutrino energy ($\langle E_\nu \rangle \sim 3.5$ GeV to p_T of 2.5 GeV/c. Current theoretical models do not completely describe the data in this previously unexplored high p_T region. The single differential cross section as a function of four momentum transfer (Q_{QE}^2) now extends to 4 GeV² with high statistics. The cross section as a function of Q_{QE}^2 shows that the tuned simulations developed by the MINERvA collaboration that agreed well with the low energy beam measurements do not agree as well with the medium energy beam measurements. Newer neutrino interaction models such as the GENIE 3 tunes are better able to simulate the high Q_{QE}^2 .

* Now at High Energy Physics/Center for Computational Excellence Department, Argonne National Lab, 9700 S Cass Ave,

Lemont, IL 60439

I. INTRODUCTION

Recent results from the neutrino oscillation experiments NOvA [1] and T2K [2] hint that charge-parity (CP) symmetry is violated in the lepton sector and favor a normal mass ordering of neutrino mass-states. Precise determination of the PNMS [3] CP violating parameter (δ_{CP}) requires new measurements with larger statistics and significantly smaller systematic uncertainties. The DUNE [4] and HyperK [5] experiments aim to measure $\delta_{CP} \neq 0$ with greater than 5 σ sensitivity at maximal δ_{CP} , which require that less than 2% of interaction rate uncertainties come from cross-section models [4]. This 2% uncertainty can be achieved with improved cross section measurements. The data presented here overlap the energy range of the DUNE experiment, although on a hydrocarbon target instead of argon.

We present results on the charge-current quasi-elastic (CCQE) process, $\bar{\nu}_\mu p \rightarrow \mu^+ n$, which is a significant component of the charged-current interactions rate [6] in the few GeV energy range. To achieve high fiducial mass, present and future neutrino experiments employ detectors made of heavier nuclei (argon in the case of DUNE and water in the case of HyperK) where nuclear processes and final state interactions (FSI) will affect the interpretation of CCQE interactions. As the primary neutrino interaction occurs within a nucleus, the pure CCQE process itself is not experimentally accessible. We instead use a CCQE-like signal definition (charged current event with no pions in the final state) based on the event topology observable outside the nucleus. Our CCQE-like definition is similar to the CC0 π definition used by other experiments [7], [8], [9]. The advantage of concentrating on CCQE-like processes is that, as a 2-body process, the full kinematics of the interaction are approximately determined from the outgoing charged lepton kinematics alone. This provides an estimate of the incoming neutrino energy, as needed for oscillation measurements, and can be applied in a consistent fashion to both neutrino and anti-neutrino interactions, despite final state differences.

This work improves upon our previous measurement in the anti-neutrino channel [10] by utilizing utilizing 20 \times statistics, background subtraction methods, and access

to an extended kinematic regions due to the higher energy beam. It complements our previous muon-neutrino cross section measurement at similar beam energy [11]. We first present the double differential cross section as a function of muon momenta (p_T and $p_{||}$) as it is largely model-independent and allows stringent tests of interaction models. We also present cross section measurements as a function of the estimated four-momentum-transfer squared variable, Q_{QE}^2 , using the CCQE hypothesis. To provide a better comparison with global neutrino energy cross sections, we present the total anti-neutrino CCQE-like cross section $\sigma(E_\nu)$ corrected from $E_{\nu(QE)}$ (neutrino energy based on CCQE hypothesis) to the true E_ν . The correction from the observable $E_{\nu(QE)}$ to E_ν is sensitive to nuclear effects and introduces additional model uncertainties.

II. THE MINERVA EXPERIMENT

The MINERvA experiment was located on-axis in the NuMI neutrino beam [12], which serves as the neutrino source. In the NuMI beamline, a 120 GeV proton beam impinges on a 1.2 meter long target to produce pions and kaons. Negatively charged mesons are then focused by two magnetic horns. The focused beam decays within a 675 meter long decay pipe to produce leptons and anti-neutrinos. Data were taken between June 2016 and February 2019.

The MINERvA detector consisted of planes of scintillating strips interleaved with nuclear targets, a central tracker region consisting only of scintillator, an electromagnetic calorimeter formed by adding lead planes and a hadronic calorimeter formed from iron plates. Muon charge and momentum measurements were provided for muons with momenta above ~ 1.5 GeV/c by the MINOS near detector [13], which was located directly behind the MINERvA detector. The data presented here are from the central tracking region of MINERvA which consisted of 108 tracking planes of scintillator composed of 88.5% Carbon, 8.2% Hydrogen and 2.5% Oxygen. The tracker could reconstruct charged tracks with a kinetic energy (T_p) threshold of ~ 120 MeV for protons.

III. EVENT SELECTION

The definition of CCQE-like process is given in our previous lower energy (LE) results [10]. Reconstructed anti-neutrino candidates with one positively charged muon, no other charged tracks and small recoil energy outside a 100 mm radius around the neutrino interaction vertex are selected. The final state muon is required to enter the downstream, magnetized MINOS near detector for charge determination and full momentum reconstruction. To match the forward MINOS acceptance, and assure that the muon charge is positive in the presence of neutrinos in the antineutrino beam, we require that the

[†] Now at Iowa State University, Ames, IA 50011, USA

[‡] now at Department of Physics and Astronomy, University of California at Davis, Davis, CA 95616, USA

[§] Now at Brookhaven National Laboratory, Upton, New York 11973-5000, USA

[¶] Now at Los Alamos National Laboratory, Los Alamos, New Mexico 87545, USA

^{**} now at Department of Physics and Astronomy, University of Mississippi, Oxford, MS 38677

^{††} Now at University of Minnesota, Minneapolis, Minnesota 55455, USA

^{‡‡} Now at Department of Physics, University of Cincinnati, Cincinnati, Ohio 45221, USA

reconstructed $\theta_\mu < 20^\circ$ and that the muon have positive charge and $p_{||}$ between 1.5 and 15 GeV/c. CCQE-like candidate events are further defined by limits on the recoil energy deposited by the outgoing hadrons. Reconstructed non-muon recoil energy is required to be less than a value that varies with Q_{QE}^2 and is similar to that of the low energy analysis [10] but has been loosened by 50 MeV due to increased backgrounds in the higher intensity ME beam. To match our detection capabilities, the CCQE-like process is defined at generator level by requiring a final state with a μ^+ with polar angle $\theta_\mu < 20^\circ$ with respect to the beam and $p_{||}$ in the range 1.5 to 15 GeV/c, no final state protons above the proton reconstruction threshold (120 MeV) and no mesons or heavier baryons. Interactions that include nuclear excitation photons below 10 MeV are allowed. This CCQE-like definition is designed to exclude non-elastic interactions such as resonances and deep-inelastic scatters, but does include interactions with multi-nucleon initial states such as 2p2h [14] and any resonant events where additional pions and nucleons are absorbed in the nucleus. In the CCQE 2-body kinematic hypothesis, the initial nucleon is assumed to be at rest with a binding energy of 30 MeV in carbon. This allows an estimate of the anti-neutrino energy $E_{\nu(QE)}$ and momentum transfer squared Q_{QE}^2 from the muon kinematics alone [10].

IV. SIMULATION

Anti-neutrino interactions are simulated using the GENIE 2.12.6 event generator [15]. This implementation of GENIE uses the relativistic Fermi Gas Model [16] with short range correlations included via a Bodek-Ritchie tail [17]. Multi-nucleon events using the Valencia model [18], [19], [20] are included. The default GENIE model is referred to as GENIE 2.12.6 in subsequent figures. The simulation used for cross section extraction is the MINERvA Tune-v1 tune described in [11]. This simulation has been tuned to match previous MINERvA data in the neutrino channel and is found to be consistent with our previous LE anti-neutrino measurement [10]. This tune includes:

- i.* Modification of non-resonant pion production rates based on a combined re-analysis of the ANL [21], [22] and BNL [23] bubble chamber data [24]. This modification reduces the non-resonant pion production by 57%. This modification has quite small effect ($< 1\%$) in this analysis and is referred to as (π tune) in Table II but not shown separately in the figures.
- ii.* A further empirical enhancement of the Valencia model based on [25] which increases integrated multi nuclear event rate by 49%. This is referred to as (Low Recoil Tune) in the figures.
- iii.* Long range correlations modeled by the random phase approximation correction based on [26] and implemented for MINERvA in [27]. This is referred to as RPA in the figures.

There is an additional suppression of pion production at low Q^2 to decrease an observed tension between data and simulation in previous experiments ([28], [29]) using an *ad hoc* fit [30]. Addition of this tune makes MINERvA Tune-v2.

The GENIE 2.12.6 model used as a basis for our full detector simulation does not include the $\Delta S = -1$ hyperon production processes [31] $\bar{\nu}_\mu + n \rightarrow \mu^+ + Y$ that contribute only in anti-neutrino scattering. These processes can contribute up to 6-8% to the total anti-neutrino scattering cross section. However, a generator level study using a more recent version of GENIE (v3.0.6) [32] that does include these processes indicates that almost all hyperon production results in either detectable tracks or significant energy deposition that are vetoed by the multiplicity and recoil selections used to define the CCQE-like data sample. Any residual hyperon processes are estimated to contribute $\sim 1\%$ to the final CCQE-like data sample.

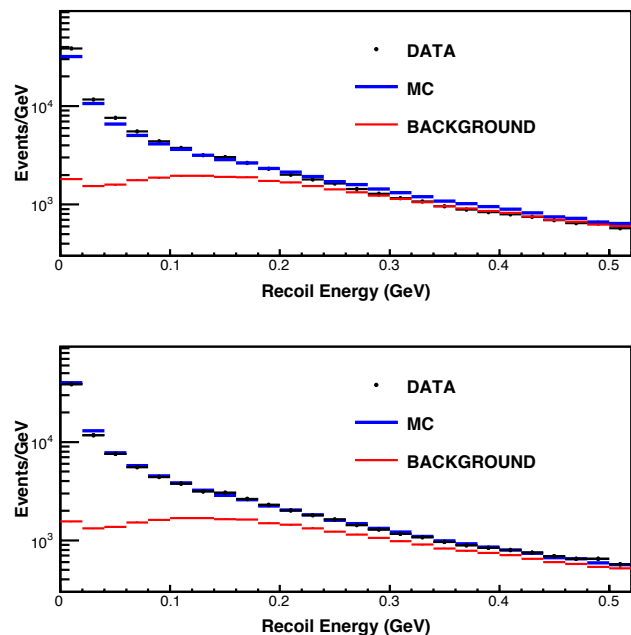


FIG. 1. The recoil energy distribution in the bin of $p_T = 0.25 - 0.4$ GeV/c, $p_{||} = 1.5 - 5$ GeV/c. The top figure shows the data compared to default simulation. The bottom figure shows the contributions of simulated signal and background after their relative contributions have been constrained to the data in the region above 100 MeV. The χ^2 of this fit is 16 for 19 degrees of freedom.

A GEANT4 [33] based full detector simulation models the response of the detector [34]. The simulation is

tuned to match test beam data [35] and overlain with random detector readouts to reproduce rate dependent backgrounds. Background contributions from non-CCQE-like processes are then estimated by fitting the reconstructed recoil distribution between 100 and 500 MeV before recoil selection to simulated signal and background samples in 14 $p_T, p_{||}$ bins. Figure 1 illustrates one of the fits for a typical $p_T, p_{||}$ bin.

The signal selection efficiency is estimated to be $\sim 70\%$ and the selected sample is 70-80% pure, with the purity falling at higher Q^2 .

A total of $635,592 \pm 1,251$ (stat.) $\pm 13,850$ (syst.) events are selected after background subtraction compared to 14,839 events in the LE sample [10]. The background subtracted sample is unfolded to the true kinematic variables using an iterative Bayesian unfolding based on the RooUnfold algorithms [36].

The sample is then corrected for geometric efficiency and normalized by the total number of protons on target (1.12×10^{21}) and the total number of nucleons in the fiducial volume of the detector (3.23×10^{30} nucleons). The total anti-neutrino flux integrated from 0 to 120 GeV is used to obtain the differential cross sections.

V. UNCERTAINTIES

Error summary related to the double differential cross section shown in figure 2 is shown in figure 7. Three major factors influence the uncertainties on this measurement. First the incoming neutrino flux has uncertainties in both overall normalization and energy dependence. The anti-neutrino flux is modeled using a GEANT4-based simulation of the target material and focusing systems. Focusing uncertainties are estimated by generating alternate fluxes where the focusing components of the beamline are shifted by $\pm 1 \sigma$ from their nominal positions. Hadron production in the simulation is modified to match thin target data-sets following the method of [37] that uses thin target data from the NA49 experiment [38] and the Barton data-sets [39]. Recent constraints from $\nu + e$ [40], $\bar{\nu} + e$ scattering [41] and inverse muon decay [42] reduce the overall flux uncertainty from $\sim 8\%$ to $\sim 5\%$. Second, substantial uncertainties related to recoil and muon reconstruction dominate the overall uncertainty budget and are estimated by varying the muon energy scale and angle, their resolutions and the neutron interaction cross section. As described in [43] the muon energy scale is corrected by 3.6% from its nominal value to resolve a discrepancy between data and the simulation. Correlations between neutrino flux parameters and muon energy scale, which result from that simultaneous fit to the energy scale and flux parameters, are accounted for, when assessing the muon energy uncertainty. Muon reconstruction induced uncertainties in the cross section range from 2-3% at low Q_{QE}^2 to $\sim 10\%$ at high Q_{QE}^2 . Uncertainties in the energy loss and detection efficiency of final-state hadrons in the MINERvA detector also in-

roduce uncertainties in the reconstruction of the recoil energy and are estimated by simulating the effects of differing hadronic interaction cross sections in the detector. The recoil response uncertainty contribution to the cross section is dominated by the model of neutron interactions and ranges from 1% at low Q_{QE}^2 to 4% at high Q_{QE}^2 .

Finally, the cross section extraction depends on proper simulation of neutrino interactions including final state processes, which are estimated by varying input parameters to the event simulations. Final state interactions (FSI) effects contribute less than 2-3% on the final cross-section uncertainty while GENIE cross-section model parameters (such as the axial mass, random phase approximation and resonance production) contribute from 1% at low Q_{QE}^2 to 6% at high Q_{QE}^2 .

Uncertainties are propagated through the “universe” method developed by the MINERvA collaboration and described in Ref. [44]. For each observable, separate histograms (“universes”) of the simulated reconstructed variable are stored for each of the several hundred sources of systematic uncertainty. For example, the reconstructed muon angle is replicated with $\pm 1\sigma$ offsets in 2 directions transverse to the beam and several GENIE parameters are similarly varied. The full analysis chain is applied to each universe independently. For the flux systematics which depend upon various beamline parameters, 500 “universes” are simulated where each universe is drawn from a distribution of focusing parameters that takes into account their uncertainties and their correlations. These beam parameters and their 1σ values are listed in [43]. The total systematic uncertainty and covariance for any observable are then estimated by summing the deviations of the modified universes from the central values provided by the simulation in quadrature [37]. Table I summarizes the significant uncertainties in the measured cross section.

VI. DISCUSSION OF RESULTS

The primary result is the measured double differential cross section in bins of muon momenta shown in Fig. 2. The MINERvA Tune v1 predictions are shown along with their components. The integrated cross section for $1.5 < p_{||} < 15$ GeV/c and $0.0 < p_T < 2.5$ GeV/c within our restricted fiducial region is $5.28 \times \pm 0.02 \pm 0.35 \times 10^{-39}$ cm²/nucleon. The relative contributions of various processes of the MINERvA Tune v1 is shown in Fig. 3. Our model predicts that the CCQE-like cross section is dominated by pure 1p1h QE and 2p2h processes. The low p_T region is dominated by QE and 2p2h processes whereas the high p_T region is dominated by QE processes only. Generally, the data lies above the simulation in almost all bins, with the excess growing as p_T increases.

Figure 4 shows the ratio of data and a suite of cross-section models to the baseline GENIE 2.12.6 which uses the Valencia 2p2h model as a function of Q_{QE}^2 . The cross-section models shown are default GENIE, the MINERvA

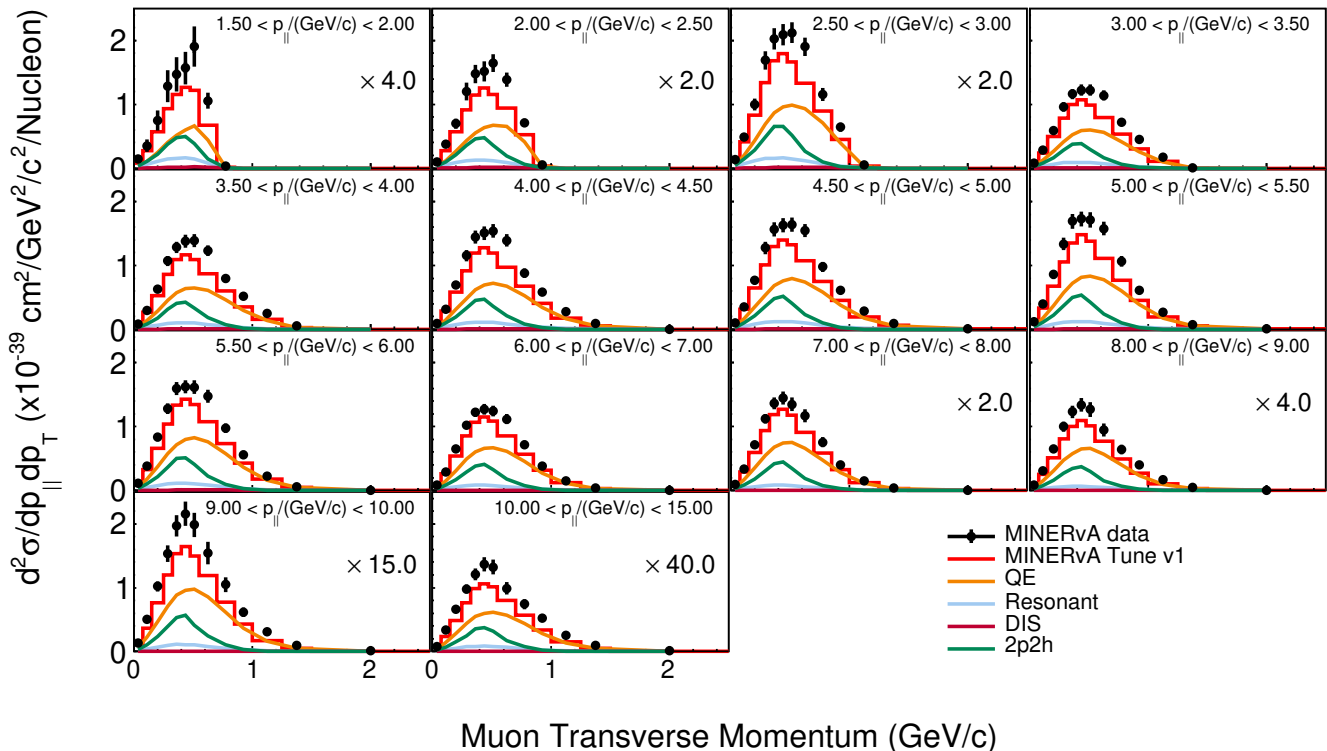


FIG. 2. The double differential CCQE-like anti-neutrino cross section as a function of muon p_T in bins of $p_{||}$. The black markers are the measured cross section and the solid lines are the model predictions of MINERvA Tune v1 and its individual components. The multipliers on the panels are the scale factors used to scale the histograms.

Quantity	Variation ($\pm 1\sigma$ from CV)	Effect on cross section (%)
Angle reconstruction	± 1 mr	0 - 2
MINOS muon energy scale	± 1.0 %	2 - 6
GEANT Neutron	± 10 %	2 - 5
Flux	focusing and hadronic interaction parameters	5
GENIE Cross Section Models	GENIE cross section parameters	1-5
GENIE 2p2h	Low recoil fit parameters	1-3
Final State Interaction Model	GENIE FSI models parameters	1-3

TABLE I. Effect of input uncertainties on the cross section extraction for $d\sigma/dQ_{QE}^2$. Uncertainties which have significant effect on final cross section are listed. The $\pm 1\sigma$ is the shift of model parameters from their central values (CV).

tunes and partial combinations of the components in the MINERvA tunes. All of the GENIE 2 models fail to reproduce the high Q_{QE}^2 behavior of the cross section. The shape of the data appears to favor models that include RPA effects while the π -tune correction appears to have little effect on the predicted rates. Recently available GENIE 3.0.6 models appear to better reproduce the high Q^2 behavior and are shown on the right hand side of Fig. 4. Comparisons are shown with 2 different cross-section model tunes [32]. The tune G18_02x_02_11a has a 2p2h model similar to that of default GENIE 2. GENIE 3 models G18_10a_02_11a and G18_10b_02_11a incorporate the default Valencia [45] model. G18_10a_02_11a uses an effective “hA” intranuclear transport model while G18_10a_02_11a incorporates the full intranuclear “hN”

transport model which includes additional processes [32]. The best χ^2 agreement among the GENIE 3 models is with model G18_10b_02_11a which incorporates the Valencia model and the “hN” model for final state interactions.

Table II lists the χ^2 for comparisons of the model variations to the 2-D $p_T, p_{||}$ cross section measurements. The χ^2 is calculated in two ways, once on the values themselves and once on the log of the values. The log method is discussed in more detail in references [10, 46] and is more robust in the presence of multiplicative normalization uncertainties.

Figure 5 shows comparisons of data to simulation for the parallel neutrino data [11] sample and this sample as a function of Q_{QE}^2 . Both ν_μ and $\bar{\nu}_\mu$ cross sections are

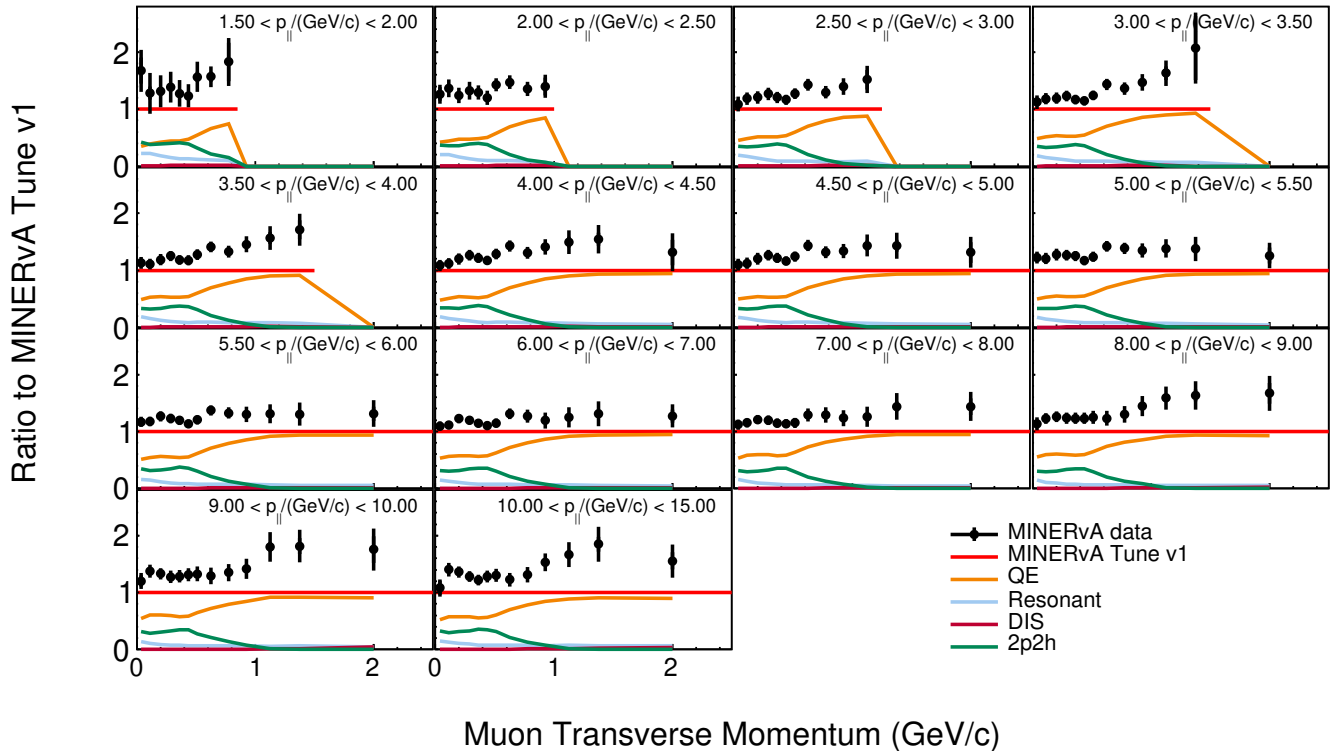


FIG. 3. Ratio of cross sections of data and various components of MINERvA Tune v1 to MINERvA Tune v1.

extracted from the same fiducial region of the MINERvA detector. The ν_μ cross section includes CCQE-like events with any number of protons, whereas the $\bar{\nu}_\mu$ requires no protons above $T_p = 120$ MeV. Only events with $p_{||}$ less than 15 GeV/c for $\bar{\nu}$ are selected to reduce the larger wrong sign neutrino contamination in the anti-neutrino beams. As the beam energy is peaked well below this threshold, this restriction has negligible effect except for a $\sim 1\%$ reduction in the highest Q_{QE}^2 bin. Signal selection cuts for the ν_μ events are given in [11].

The left panel on Fig. 6 shows various models and data as a function of true neutrino energy. On the right panel, green data points and lines show the cross section and MINERvA models corrected to all θ_μ and T_p (kinetic energy of the final state proton) for easier comparison to inclusive models and other experiments. Both panels show that models underpredict the data.

A. Summary

We have presented the anti-neutrino CCQE-like cross section measured with the NuMI $< E_\nu > \sim 6$ GeV beam in the MINERvA detector. The measurement extends our past measurements in the anti-neutrino channel made in the lower neutrino energy beam and complements the neutrino cross section measurement at higher energy. We have extended the measurement to Q_{QE}^2 of 4 GeV².

Model	χ^2 - linear	χ^2 - log
GENIE 2.12.6 Tunes		
MINERvA Tune v1	362.6	580.4
MINERvA Tune v2	364.4	601.4
GENIE w/o 2p2h	226.5	473.2
GENIE (Default)	346.4	550.6
GENIE+ π tune	354.3	568.5
GENIE+RPA	230.0	406.7
GENIE+RPA+ π tune	231.7	414.6
GENIE+Low Recoil Tune	755.4	1059.4
GENIE+Low Recoil Tune+RPA	361.2	570.0
GENIE+Low Recoil Tune+ π tune	760.6	1081.8
GENIE 3.0.6 Tunes		
GENIE 3.0.6 G18_02a_02_11a	602.9	865.0
GENIE 3.0.6 G18_02b_02_11a	586.9	878.3
GENIE 3.0.6 G18_10a_02_11a	353.1	447.5
GENIE 3.0.6 G18_10b_02_11a	312.8	421.7

TABLE II. $p_{||} - p_{\perp}$ χ^2 between data and model variants derived from GENIE. The number of degrees of freedom is 171. Both the χ^2 between the values and between the logs of the values are listed.

These measurements indicate that none of the variations of GENIE v2 based on the MINERvA low energy data are sufficient to describe the MINERvA medium energy data. However, GENIE v3 models appear to better describe the data especially in the high Q_{QE}^2 region which is

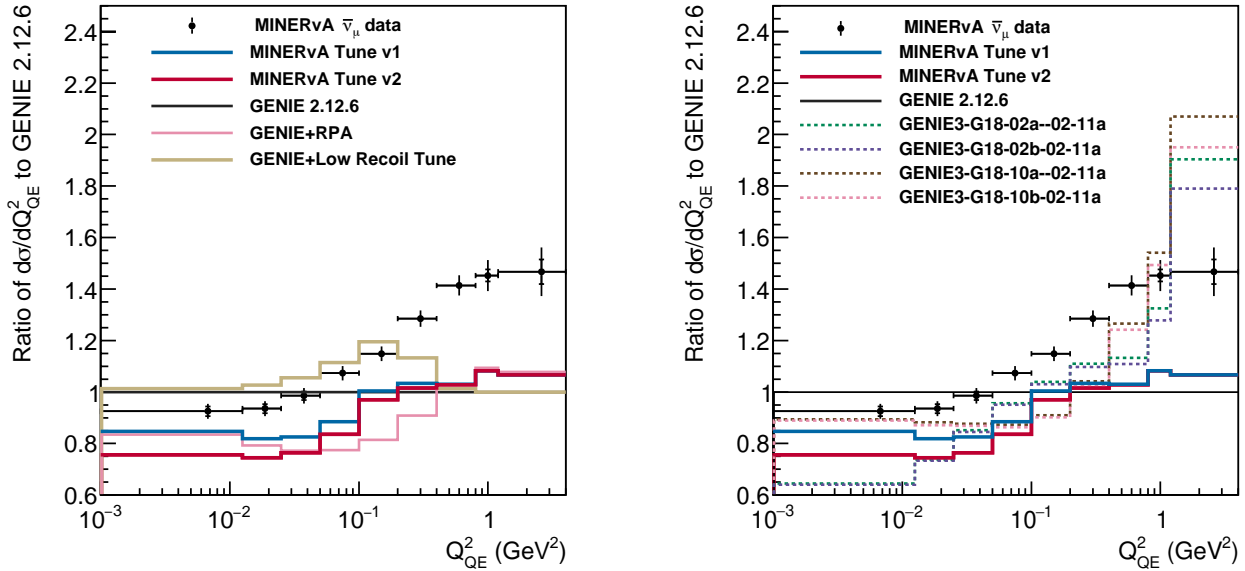


FIG. 4. Comparisons of the cross section predicted by various tunes applied on GENIE with respect to the baseline GENIE 2.12.6 (black) as a function of Q_{QE}^2 (left). MINERvA Tune v1 (blue) is the standard simulation tuned to the MINERvA low energy data. MINERvA Tune v2 (red) is MINERvA Tune v1 with the non-resonant pions suppressed in the low Q_{QE}^2 region [30]. The remaining curves show the effect of enabling different corrections to the base model. The plots on the right show comparisons of cross sections predictions for GENIE v3.0.6 (dotted lines) with the MINERvA tuned GENIE predictions. Inner ticks in the data are statistical and the outer ticks are the systematic uncertainties.

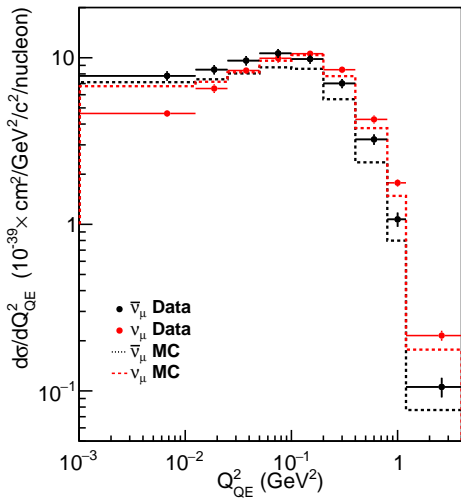


FIG. 5. Measured (data points) and MINERvA Tune v1 prediction (dotted lines) of CCQE-like $d\sigma/dQ_{QE}^2$ for neutrinos (red) and anti-neutrinos (black) extracted with the NuMI neutrino energy ~ 6 GeV.

dominated by the QE process. This high statistics double differential cross section provides useful model inputs for future neutrino oscillation experiments. Tables of values

are available in the supplemental materials [47].

ACKNOWLEDGMENTS

This document was prepared by members of the MINERvA Collaboration using the resources of the Fermi National Accelerator Laboratory (Fermilab), a U.S. Department of Energy, Office of Science, HEP User Facility. Fermilab is managed by Fermi Research Alliance, LLC (FRA), acting under Contract No. DE-AC02-07CH11359. These resources included support for the MINERvA construction project, and support for construction also was granted by the United States National Science Foundation under Award No. PHY-0619727 and by the University of Rochester. Support for participating scientists was provided by NSF and DOE (USA); by CAPES and CNPq (Brazil); by CoNaCyT (Mexico); by Proyecto Basal FB 0821, CONICYT PIA ACT1413, and Fondecyt 3170845 and 11130133 (Chile); by CONCYTEC (Consejo Nacional de Ciencia, Tecnología e Innovación Tecnológica), DGI-PUCP (Dirección de Gestión de la Investigación - Pontificia Universidad Católica del Peru), and VRI-UNI (Vice-Rectorate for Research of National University of Engineering) (Peru); NCN Opus Grant No. 2016/21/B/ST2/01092 (Poland); by Science and Technology Facilities Council (UK). We thank the MINOS Collaboration for use of its near detector data.

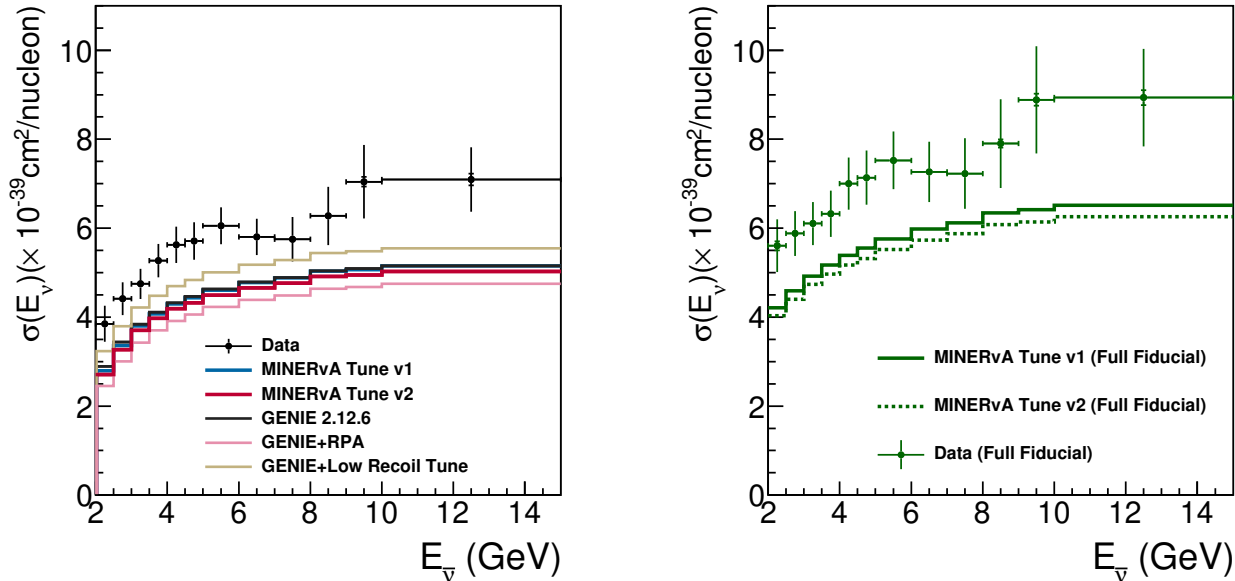


FIG. 6. CCQE-like cross section as a function of true $\bar{\nu}$ energy. The black data points on the left pane use our fiducial final state definition with $\theta_\mu < 20^\circ$ and $T_p < 120$ MeV. The green points on the right pane are data and the MINERvA tunes v1 and v2 model predictions (straight and dotted lines) for the total cross section with those fiducial selections removed.

Finally, we thank the staff of Fermilab for support of the beam line, the detector, and computing infrastructure.

-
- [1] M. A. Acero *et al.* (NOvA), *Phys. Rev. D* **106**, 032004 (2022), [arXiv:2108.08219 \[hep-ex\]](#).
- [2] K. Abe *et al.* (T2K), *Nature* **580**, 339 (2020), [Erratum: *Nature* 583, E16 (2020)], [arXiv:1910.03887 \[hep-ex\]](#).
- [3] R. L. *et al.*. Workman (Particle Data Group), *PTEP* **2022**, 083C01 (2022).
- [4] B. Abi *et al.* (DUNE), *Eur. Phys. J. C* **80**, 978 (2020), [arXiv:2006.16043 \[hep-ex\]](#).
- [5] M. Yokoyama (Hyper-Kamiokande Proto), in *Prospects in Neutrino Physics* (2017) [arXiv:1705.00306 \[hep-ex\]](#).
- [6] J. A. Formaggio and G. P. Zeller, *Rev. Mod. Phys.* **84**, 1307 (2012).
- [7] K. Abe *et al.* (T2K), *Phys. Rev. D* **101**, 112004 (2020), [arXiv:2004.05434 \[hep-ex\]](#).
- [8] A. A. Aguilar-Arevalo *et al.* (MiniBooNE), *Phys. Rev. D* **88**, 032001 (2013), [arXiv:1301.7067 \[hep-ex\]](#).
- [9] A. Papadopoulou, *PoS NuFact2021*, 189 (2022).
- [10] C. Patrick *et al.* (MINERvA), *Phys. Rev. D* **97**, 052002 (2018), [arXiv:1801.01197 \[hep-ex\]](#).
- [11] M. Carneiro *et al.* (MINERvA), *Phys. Rev. Lett.* **124**, 121801 (2020), [arXiv:1912.09890 \[hep-ex\]](#).
- [12] P. Adamson *et al.*, *Nucl. Instrum. Meth. A* **806**, 279 (2016), [arXiv:1507.06690](#).
- [13] S. G. Wojcicki, *Nuclear Physics B - Proceedings Supplements* **77**, 182 (1999).
- [14] R. Subedi *et al.*, *Science* **320**, 1476 (2008), [arXiv:0908.1514 \[nucl-ex\]](#).
- [15] C. Andreopoulos *et al.*, *The GENIE Neutrino Monte Carlo Generator: Physics and User Manual* (2015), [arXiv:1510.05494 \[hep-ph\]](#).
- [16] R. S. and E.J. Moniz, *Nucl. Phys.* **B43**, 605 (1972).
- [17] A. Bodek and J. Ritchie, *Phys. Rev. D* **23**, 1070 (1981).
- [18] J. Nieves, J. E. Amaro, and M. Valverde, *Phys. Rev. C* **70**, 055503 (2004), [Erratum: *Phys. Rev. C* 72,019902(2005)], [arXiv:nucl-th/0408005](#).
- [19] R. Gran, J. Nieves, F. Sanchez, and M. Vicente Vacas, *Phys. Rev. D* **88**, 113007 (2013), [arXiv:1307.8105 \[hep-ph\]](#).
- [20] J. Schwehr, D. Cherdack, and R. Gran, GENIE implementation of IFIC Valencia model for QE-like 2p2h neutrino-nucleus cross section (2016), [arXiv:1601.02038 \[hep-ph\]](#).
- [21] S. Barish *et al.*, *Phys. Rev. D* **16**, 3103 (1977).
- [22] N. Baker, P. Connolly, S. Kahn, M. Murtagh, R. Palmer, N. Samios, and M. Tanaka, *Phys. Rev. D* **25**, 617 (1982).
- [23] K. M. Graczyk, J. Żmuda, and J. T. Sobczyk, *Phys. Rev. D* **90**, 093001 (2014), [arXiv:1407.5445 \[hep-ph\]](#).
- [24] P. Rodrigues, C. Wilkinson, and K. McFarland, *Eur. Phys. J. C* **76**, 474 (2016), [arXiv:1601.01888 \[hep-ex\]](#).
- [25] P. Rodrigues *et al.* (MINERvA), *Phys. Rev. Lett.* **116**, 071802 (2016), [Addendum: *Phys.Rev.Lett.* 121, 209902 (2018)], [arXiv:1511.05944 \[hep-ex\]](#).
- [26] J. G. Morfin, J. Nieves, and J. T. Sobczyk, *Adv. High Energy Phys.* **2012**, 934597 (2012), [arXiv:1209.6586 \[hep-ex\]](#).
- [27] R. Gran, Model Uncertainties for Valencia RPA Effect for MINERvA (2017), [arXiv:1705.02932](#).

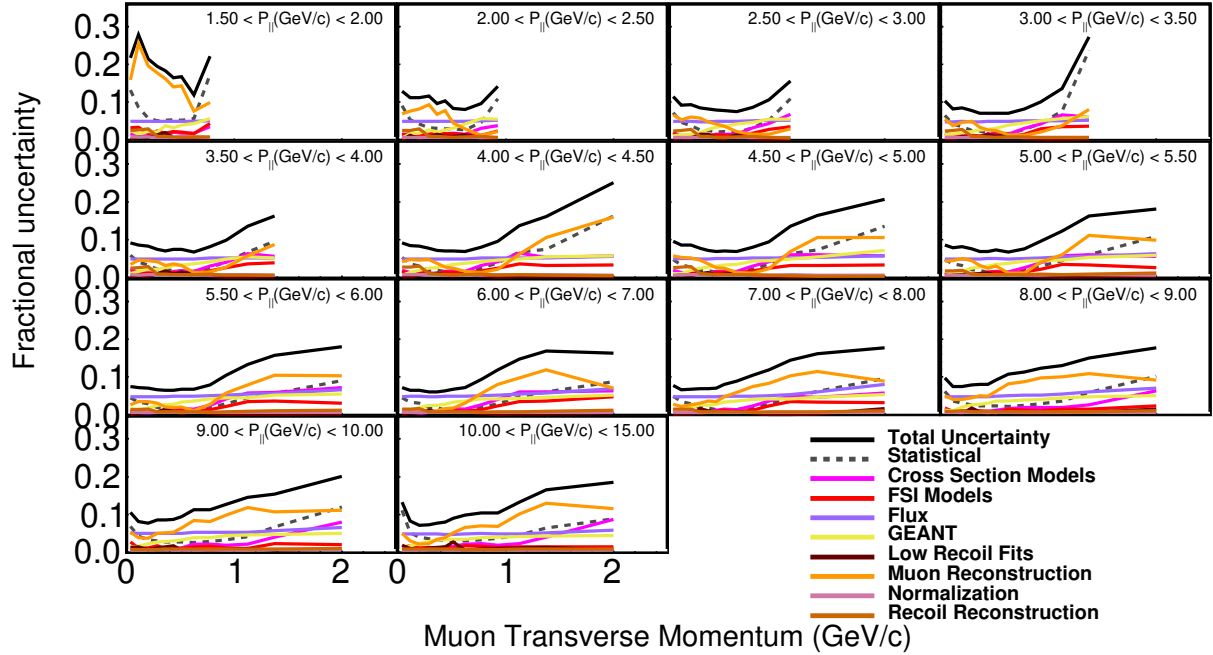


FIG. 7. Summary of uncertainties on the $p_T, p_{||}$ cross sections shown in Fig. 2.

- [28] P. Adamson *et al.* (MINOS), *Phys. Rev. D* **76**, 072005 (2007), [arXiv:0706.0437 \[hep-ex\]](#).
- [29] E. Paschos, M. Sakuda, I. Schienbein, and J. Yu, *Nucl. Phys. B Proc. Suppl.* **139**, 125 (2005), [arXiv:hep-ph/0408185](#).
- [30] P. Stowell *et al.* (MINERvA), *Phys. Rev. D* **100**, 072005 (2019), [arXiv:1903.01558 \[hep-ex\]](#).
- [31] A. Pais, *Annals of Physics* **63**, 361 (1971).
- [32] J. Tena-Vidal *et al.* (GENIE), *Phys. Rev. D* **104**, 072009 (2021), [arXiv:2104.09179 \[hep-ph\]](#).
- [33] S. A. *et al.*, *Nuclear Instruments and Methods in Physics Research Section A: Accelerators, Spectrometers, Detectors and Associated Equipment* **506**, 250 (2003).
- [34] L. Aliaga *et al.* (MINERvA Collaboration), *Nucl. Instrum. Meth. A* **789**, 28 (2015), [arXiv:1501.06431 \[physics.ins-det\]](#).
- [35] L. Aliaga *et al.* (MINERvA), *Nucl. Instrum. Meth. A* **789**, 28 (2015), [arXiv:1501.06431 \[physics.ins-det\]](#).
- [36] G. D'Agostini, *Nucl. Instrum. Meth. A* **362**, 487 (1995).
- [37] L. Aliaga *et al.* (MINERvA Collaboration), *Phys. Rev. D* **94**, 092005 (2016), [Addendum: *Phys. Rev. D* 95,no.3,039903(2017)], [arXiv:1607.00704](#).
- [38] G. Stefanek (NA49, NA61/SHINE), *Nucl. Part. Phys. Proc.* **273-275**, 2596 (2016), [arXiv:1411.2396 \[nucl-ex\]](#).
- [39] D. S. Barton *et al.*, *Phys. Rev. D* **27**, 2580 (1983).
- [40] E. Valencia *et al.* (MINERvA), *Phys. Rev. D* **100**, 092001 (2019), [arXiv:1906.00111 \[hep-ex\]](#).
- [41] L. Zazueta *et al.* (MINERvA), (2022), [arXiv:2209.05540 \[hep-ex\]](#).
- [42] D. Ruterbories *et al.* (MINERvA), *Phys. Rev. D* **104**, 092010 (2021), [arXiv:2107.01059 \[hep-ex\]](#).
- [43] A. Bashyal *et al.* (MINERvA), *JINST* **16**, P08068, [arXiv:2104.05769 \[hep-ex\]](#).
- [44] B. Messerly *et al.* (MINERvA), *EPJ Web Conf.* **251**, 03046 (2021), [arXiv:2103.08677 \[hep-ex\]](#).
- [45] J. Nieves, I. Ruiz Simo, and M. J. Vicente Vacas, *Phys. Rev. C* **83**, 045501 (2011), [arXiv:1102.2777 \[hep-ph\]](#).
- [46] A. D. Carlson *et al.*, *Nucl. Data Sheets* **110**, 3215 (2009).
- [47] See Supplemental Material at [URL_will_be_inserted_by_publisher](#) for numerical tables and details of the fractional uncertainties.

SUPPLEMENTAL MATERIAL

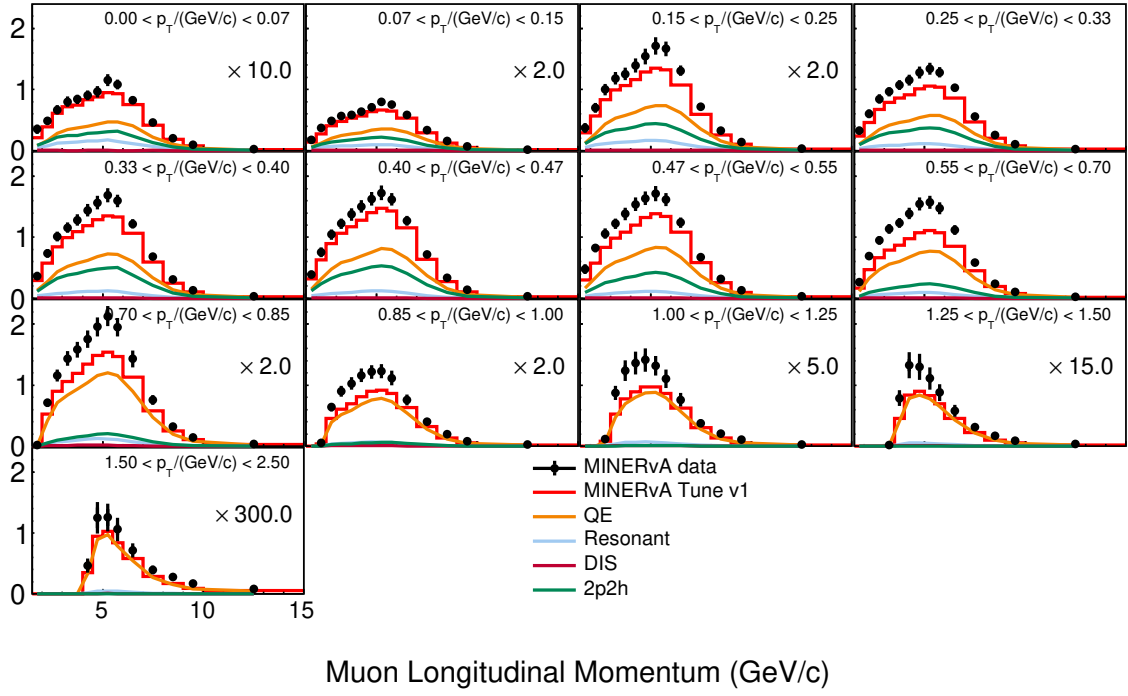


FIG. 1. Double differential cross-section as a function of muon longitudinal momentum in bins of muon transverse momentum.

TABLE I. Double differential cross-section as a function of muon kinematics. The horizontal rows are muon transverse momentum (p_T GeV/c) and vertical columns are muon longitudinal momentum ($p_{||}$ GeV/c). The cross-section is in units of $10^{-42}/\nu/\text{cm}^2/\text{nucleon}$.

$p_{\perp}(\text{GeV}/c)$	0.000–0.075	0.075–0.150	0.150–0.250	0.250–0.325	0.325–0.400	0.400–0.475	0.475–0.550	0.550–0.700	0.700–0.850	0.850–1.000	1.000–1.250	1.250–1.500	1.500–2.500
$p_{ }(\text{GeV}/c)$													
1.50 – 2.00	34.80	87.53	186.21	321.42	367.13	392.04	476.68	264.14	8.05	0.00	0.00	0.00	0.00
2.00 – 2.50	48.47	186.69	349.23	602.37	738.48	756.87	822.70	695.09	355.36	25.42	0.00	0.00	0.00
2.50 – 3.00	66.62	241.47	500.30	845.35	1014.21	1046.52	1060.81	950.51	578.21	320.37	23.93	0.00	0.00
3.00 – 3.50	80.00	282.47	591.26	961.60	1159.24	1222.45	1223.13	1137.83	718.16	449.93	174.73	1.19	0.00
3.50 – 4.00	83.76	291.08	627.36	1070.06	1284.11	1376.35	1386.07	1235.08	791.10	513.79	248.32	52.48	0.00
4.00 – 4.50	90.34	316.76	694.72	1153.20	1442.43	1505.88	1541.87	1391.40	878.71	579.92	272.61	88.44	1.56
4.50 – 5.00	96.22	353.75	770.51	1276.87	1568.53	1630.59	1640.44	1547.76	979.21	608.40	282.83	86.56	4.17
5.00 – 5.50	115.05	398.03	857.27	1338.02	1691.26	1727.89	1715.08	1576.76	1066.05	614.32	263.74	74.03	4.18
5.50 – 6.00	108.43	377.97	832.65	1277.87	1596.39	1622.68	1617.92	1473.93	975.17	558.88	220.93	58.74	3.53
6.00 – 7.00	82.77	291.11	653.83	1024.53	1221.32	1272.45	1243.11	1117.65	714.95	378.01	151.71	38.69	2.37
7.00 – 8.00	46.06	167.01	358.53	560.44	681.25	723.62	674.59	585.35	377.21	199.39	75.64	21.01	1.33
8.00 – 9.00	20.32	76.60	161.47	249.80	307.53	335.20	316.97	236.63	160.93	99.16	41.28	11.17	0.94
9.00 – 10.00	9.02	33.67	68.17	101.95	131.29	143.88	132.28	102.71	69.96	41.05	20.78	6.27	0.57
10.00 – 15.00	1.84	8.40	16.66	24.50	30.21	34.12	33.11	24.76	18.57	13.05	6.40	2.36	0.29

TABLE II. Statistical uncertainties on the double differential cross-section as a function of muon kinematics. The horizontal rows are muon transverse momentum (p_T GeV/c) and vertical columns are muon longitudinal momentum ($p_{||}$ GeV/c). The cross-section is in units of $10^{-42}/\nu/\text{cm}^2/\text{nucleon}$.

p_{\perp} (GeV/c)	0.000–0.075	0.075–0.150	0.150–0.250	0.250–0.325	0.325–0.400	0.400–0.475	0.475–0.550	0.550–0.700	0.700–0.850	0.850–1.000	1.000–1.250	1.250–1.500	1.500–2.500
$p_{ }$ (GeV/c)													
1.50 – 2.00	4.58	7.52	10.77	16.35	19.07	20.81	24.96	14.83	1.39	0.00	0.00	0.00	0.00
2.00 – 2.50	4.41	9.97	14.73	19.50	23.05	21.70	24.33	18.56	16.32	2.78	0.00	0.00	0.00
2.50 – 3.00	4.79	11.10	18.58	22.54	25.57	22.18	23.12	18.51	18.53	16.46	2.62	0.00	0.00
3.00 – 3.50	5.16	11.80	20.69	23.49	26.96	22.56	22.88	18.88	20.10	19.64	13.22	0.28	0.00
3.50 – 4.00	4.94	11.51	20.53	23.51	26.81	23.10	23.62	18.85	20.40	20.92	16.58	4.97	0.00
4.00 – 4.50	4.81	11.23	21.21	23.05	27.58	22.87	23.46	19.15	21.08	22.10	18.14	6.55	0.25
4.50 – 5.00	4.52	11.40	21.13	23.90	27.33	22.24	22.62	19.46	21.57	22.06	17.88	6.25	0.56
5.00 – 5.50	5.46	14.01	26.23	26.83	32.29	22.94	23.30	19.85	21.06	18.18	11.77	4.37	0.46
5.50 – 6.00	4.82	12.39	24.35	24.57	28.67	20.69	21.03	17.54	18.18	16.12	9.75	3.33	0.32
6.00 – 7.00	3.75	9.85	20.28	20.05	22.61	15.49	15.02	13.12	13.58	10.93	7.14	2.32	0.21
7.00 – 8.00	2.28	5.72	10.60	10.71	12.37	10.02	9.08	7.56	7.20	5.55	3.42	1.32	0.13
8.00 – 9.00	1.27	2.81	4.92	6.44	7.26	7.77	7.22	5.07	3.91	2.88	1.51	0.66	0.10
9.00 – 10.00	0.62	1.42	2.22	3.05	3.59	3.97	3.64	2.62	2.02	1.35	0.85	0.42	0.07
10.00 – 15.00	0.20	0.44	0.66	0.87	0.97	1.08	1.05	0.75	0.62	0.48	0.29	0.15	0.03

TABLE III. Systematic uncertainties on the double differential cross-section as a function of muon kinematics. The horizontal rows are muon transverse momentum (p_T GeV/c) and vertical columns are muon longitudinal momentum ($p_{||}$ GeV/c). The cross-section is in units of $10^{-42}/\nu/\text{cm}^2/\text{nucleon}$.

p_{\perp} (GeV/c)	0.000–0.075	0.075–0.150	0.150–0.250	0.250–0.325	0.325–0.400	0.400–0.475	0.475–0.550	0.550–0.700	0.700–0.850	0.850–1.000	1.000–1.250	1.250–1.500	1.500–2.500
$p_{ }$ (GeV/c)													
1.50 – 2.00	6.04	23.21	38.49	60.34	64.46	60.81	75.58	27.57	1.11	0.00	0.00	0.00	0.00
2.00 – 2.50	4.44	18.45	36.05	66.91	67.14	75.03	63.91	52.42	29.96	2.31	0.00	0.00	0.00
2.50 – 3.00	5.97	19.04	42.70	68.16	78.25	80.20	78.44	68.50	46.42	29.52	2.68	0.00	0.00
3.00 – 3.50	6.50	19.70	45.85	71.42	77.29	82.66	82.29	78.03	55.59	41.02	19.64	0.16	0.00
3.50 – 4.00	5.89	21.91	47.93	74.90	85.99	99.87	99.81	81.16	60.44	45.56	29.26	6.95	0.00
4.00 – 4.50	6.68	23.94	53.81	86.35	99.56	101.85	105.47	93.32	67.28	50.39	32.52	12.70	0.30
4.50 – 5.00	7.99	28.12	62.09	94.91	107.85	110.15	111.73	102.83	74.93	52.64	33.81	12.66	0.65
5.00 – 5.50	8.22	27.99	64.30	96.84	111.34	115.55	121.51	104.27	78.08	55.42	30.25	11.15	0.60
5.50 – 6.00	6.54	24.06	53.83	81.16	98.91	103.52	107.64	97.21	75.21	56.57	27.84	8.65	0.55
6.00 – 7.00	4.56	15.90	36.88	58.66	69.59	79.80	82.01	79.70	65.54	43.47	21.16	6.07	0.33
7.00 – 8.00	2.77	9.43	21.66	36.78	45.28	49.97	53.69	51.13	38.79	22.91	10.41	3.15	0.20
8.00 – 9.00	1.51	5.03	11.05	18.51	23.62	25.83	28.14	25.05	17.89	11.93	5.15	1.54	0.14
9.00 – 10.00	0.73	2.32	4.72	8.09	10.62	11.86	11.95	11.31	7.55	5.03	2.90	0.87	0.09
10.00 – 15.00	0.14	0.53	1.00	1.56	2.12	2.51	2.79	2.33	1.82	1.26	0.79	0.36	0.05

TABLE IV. Total uncertainties on the double differential cross-section as a function of muon kinematics. The horizontal rows are muon transverse momentum (p_T GeV/c) and vertical columns are muon longitudinal momentum ($p_{||}$ GeV/c). The cross-section is in units of $10^{-42}/\nu/\text{cm}^2/\text{nucleon}$.

p_{\perp} (GeV/c)	0.000–0.075	0.075–0.150	0.150–0.250	0.250–0.325	0.325–0.400	0.400–0.475	0.475–0.550	0.550–0.700	0.700–0.850	0.850–1.000	1.000–1.250	1.250–1.500	1.500–2.500
$p_{ }$ (GeV/c)													
1.50 – 2.00	7.58	24.40	39.97	62.51	67.22	64.27	79.59	31.31	1.78	0.00	0.00	0.00	0.00
2.00 – 2.50	6.25	20.97	38.94	69.69	70.99	78.11	68.38	55.61	34.12	3.61	0.00	0.00	0.00
2.50 – 3.00	7.65	22.03	46.56	71.79	82.32	83.21	81.77	70.95	49.98	33.79	3.75	0.00	0.00
3.00 – 3.50	8.30	22.96	50.30	75.18	81.86	85.69	85.42	80.28	59.11	45.48	23.67	0.32	0.00
3.50 – 4.00	7.69	24.75	52.14	78.51	90.08	102.51	102.56	83.32	63.79	50.13	33.63	8.54	0.00
4.00 – 4.50	8.23	26.44	57.84	89.38	103.31	104.38	108.04	95.27	70.50	55.02	37.23	14.28	0.39
4.50 – 5.00	9.18	30.34	65.58	97.87	111.26	112.37	114.00	104.66	77.98	57.08	38.24	14.12	0.86
5.00 – 5.50	9.87	31.30	69.45	100.49	115.93	117.81	123.73	106.14	80.87	58.32	32.46	11.98	0.76
5.50 – 6.00	8.13	27.06	59.08	84.80	102.99	105.57	109.68	98.78	77.37	58.82	29.50	9.27	0.64
6.00 – 7.00	5.91	18.70	42.09	61.99	73.17	81.29	83.38	80.77	66.93	44.83	22.33	6.50	0.39
7.00 – 8.00	3.59	11.03	24.12	38.31	46.94	50.96	54.45	51.69	39.46	23.57	10.96	3.41	0.23
8.00 – 9.00	1.97	5.76	12.09	19.60	24.71	26.98	29.05	25.56	18.31	12.27	5.37	1.67	0.17
9.00 – 10.00	0.95	2.72	5.22	8.64	11.21	12.51	12.50	11.61	7.82	5.21	3.02	0.96	0.11
10.00 – 15.00	0.24	0.69	1.20	1.78	2.33	2.73	2.99	2.44	1.92	1.35	0.84	0.39	0.05

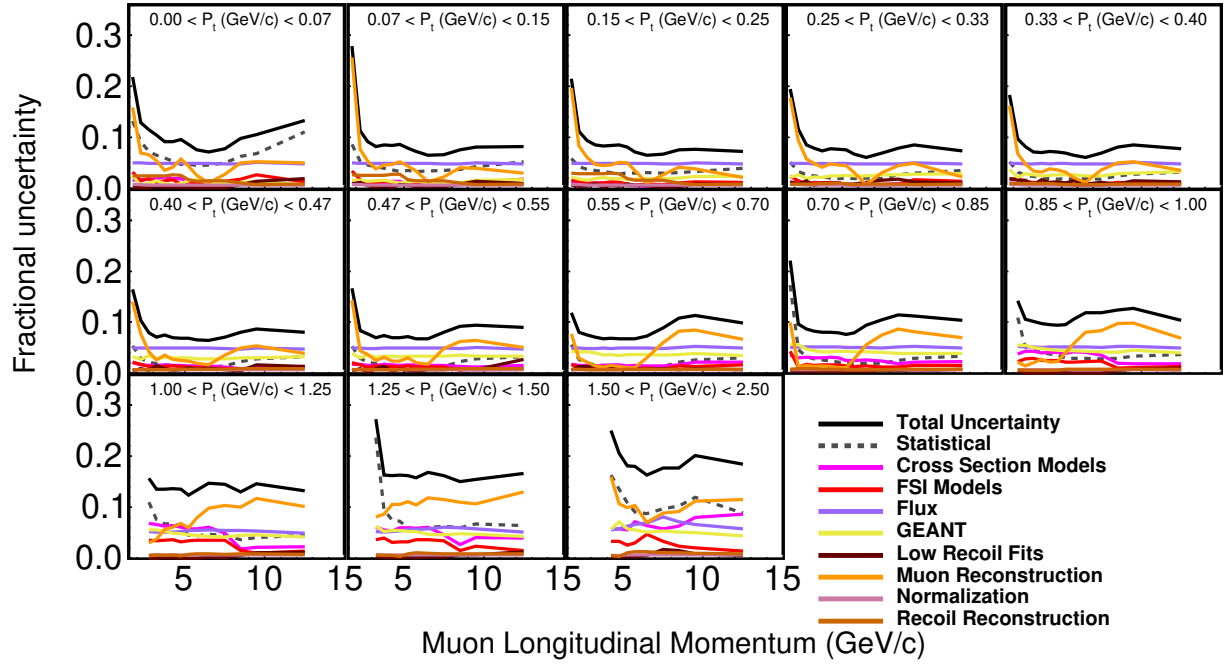


FIG. 2. Summary of fractional uncertainties on the cross-section as a function of muon longitudinal momentum in bins of muon transverse momentum.

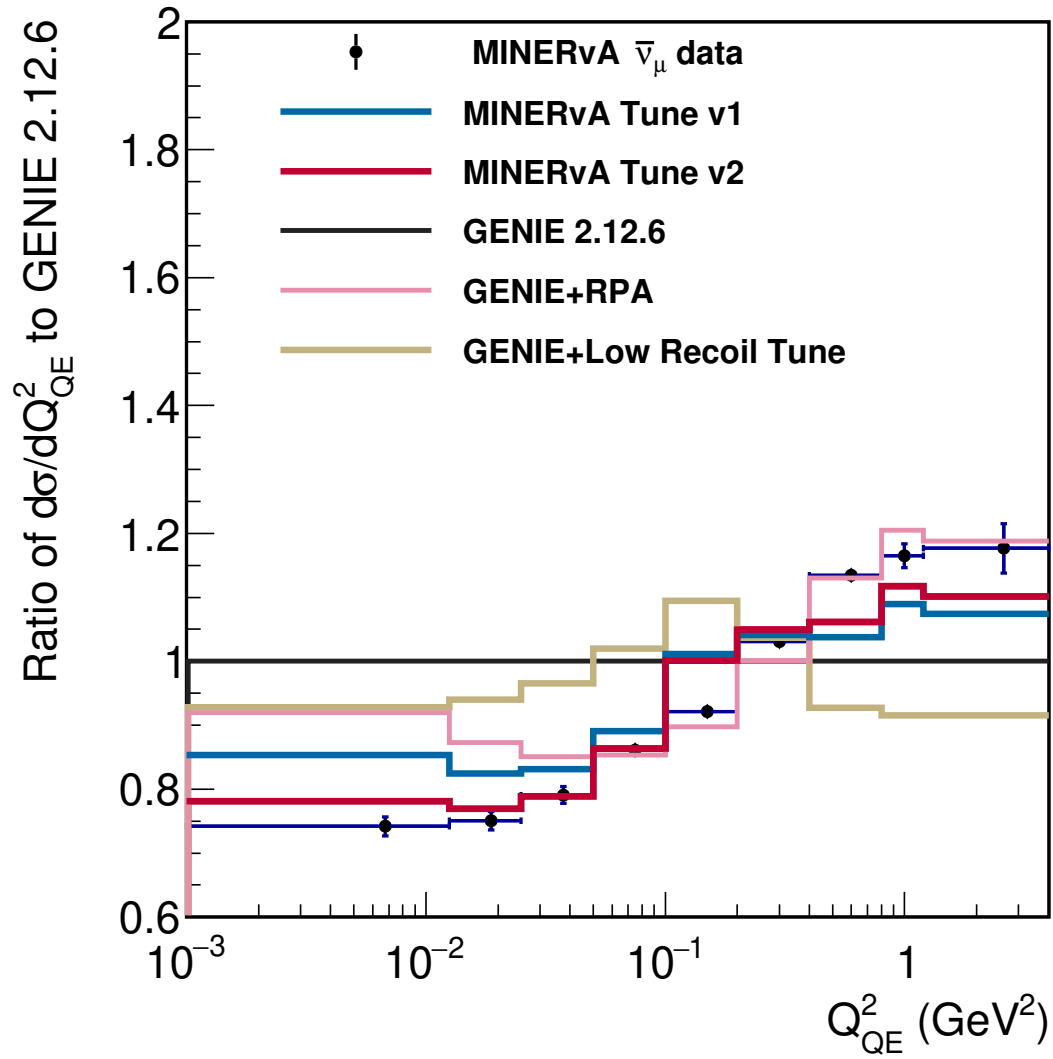


FIG. 3. Comparisons of the cross section shapes predicted by various tunes applied on GENIE with respect to baseline GENIE 2.12.6 (black) as a function of Q_{QE}^2 . The cross sections are area normalized before taking the ratio for the shape comparison.

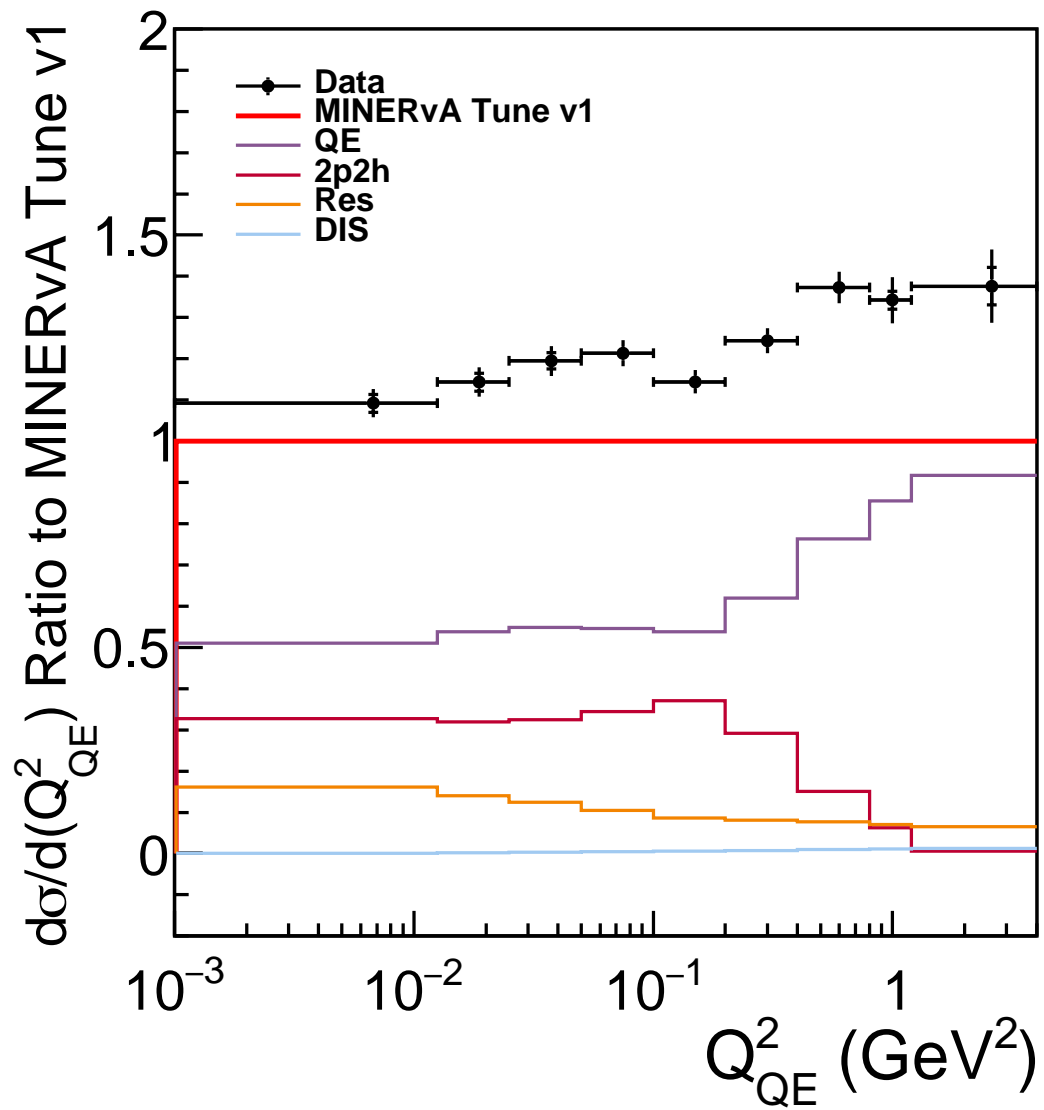


FIG. 4. Ratio of measured and various components of MINERvA Tune v1 to MINERvA Tune v1

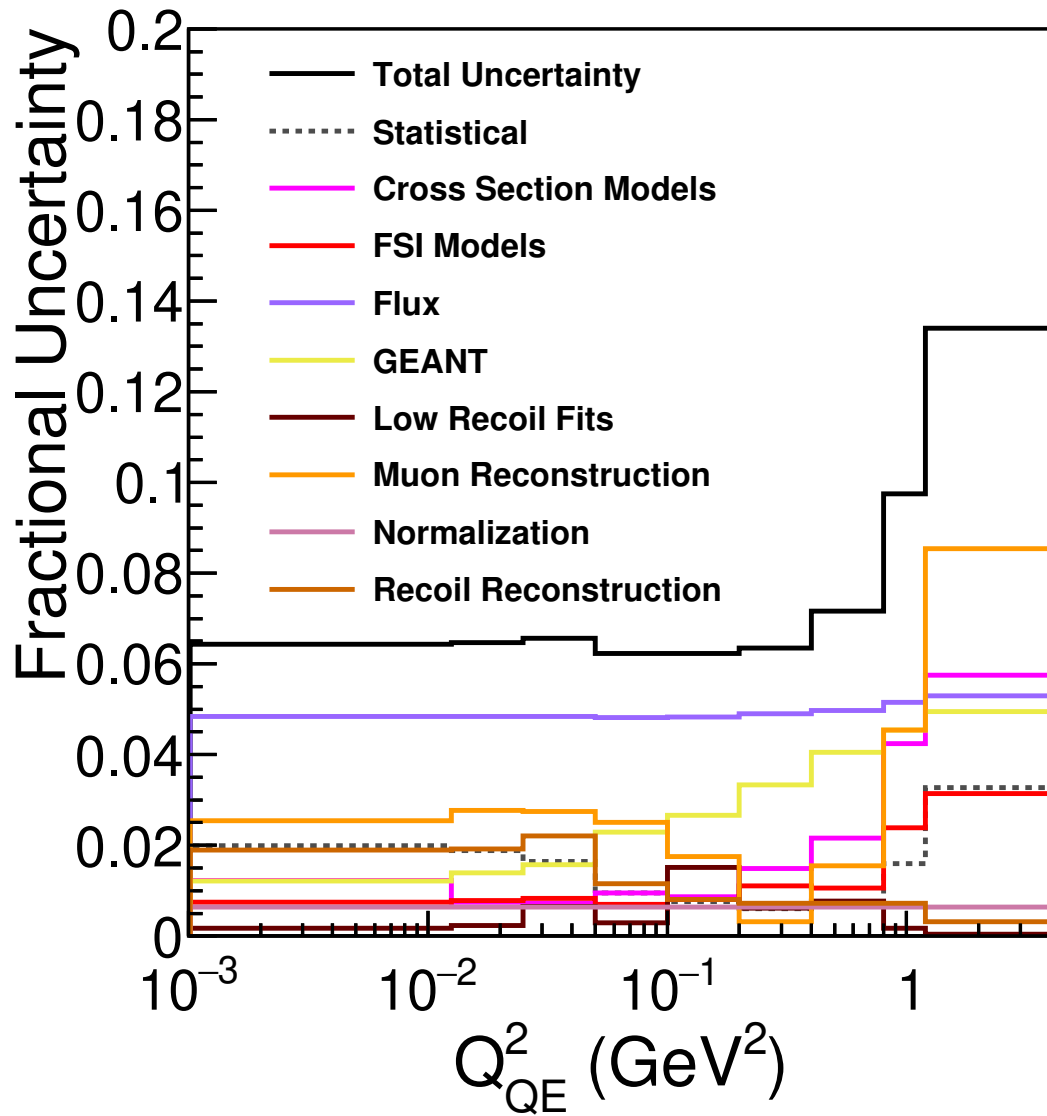


FIG. 5. Summary of fractional uncertainties on the differential cross-section as a function of Q_{QE}^2 hypothesis.

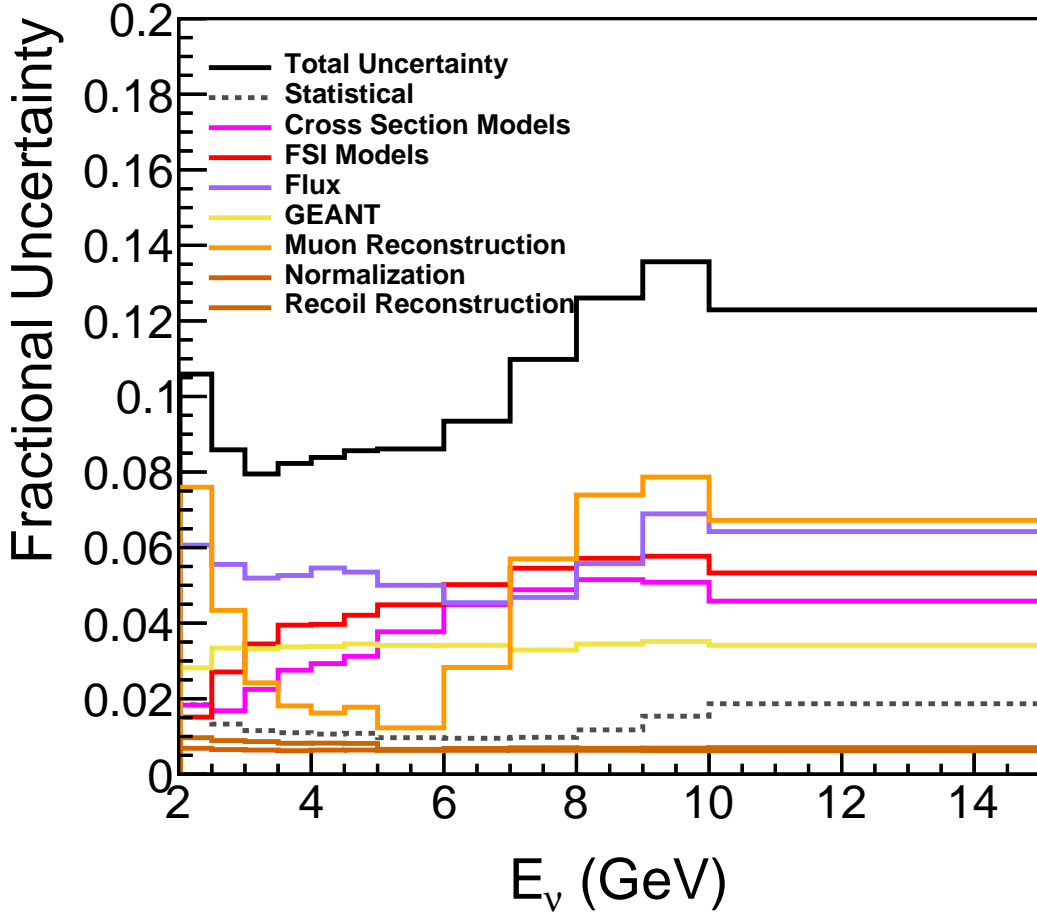


FIG. 6. Summary of fractional uncertainties on the full fiducial cross-section as a function of true neutrino energy.

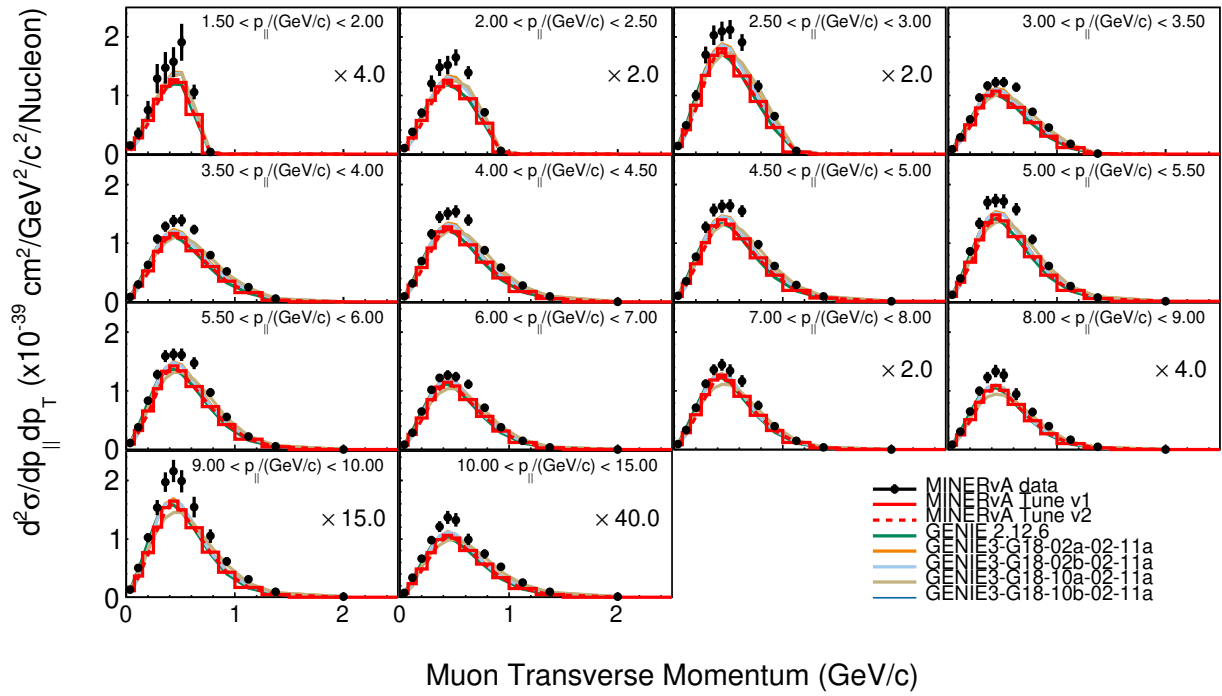


FIG. 7. Double differential cross section as a function of muon transverse momentum in bins of muon longitudinal momentum shown for GENIE 2 and tuned models along with GENIE 3 models.

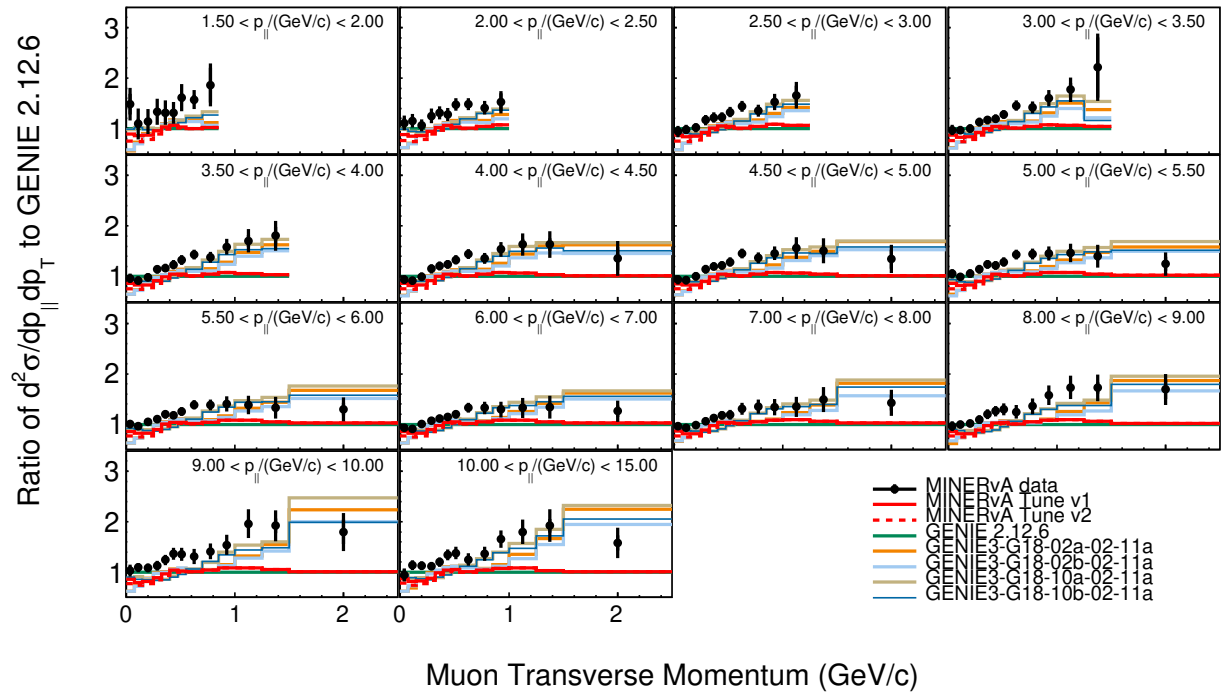


FIG. 8. Ratios of double differential cross sections to GENIE 2.12.6 as a function of muon transverse momentum in bins of muon longitudinal momentum shown for GENIE 2 and tuned models along with GENIE 3 (v3.0.6) models.

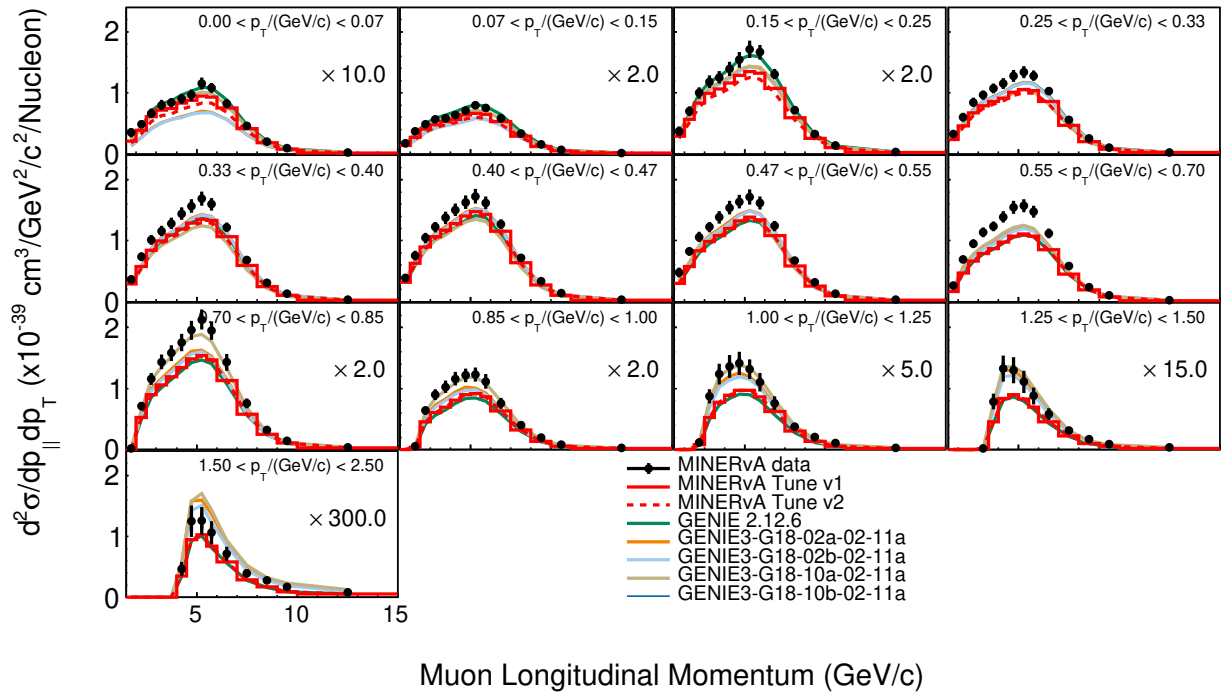


FIG. 9. Double differential cross section as a function of muon longitudinal momentum in bins of muon transverse momentum shown for GENIE 2 and tuned models along with GENIE 3 (v3.0.6) models.

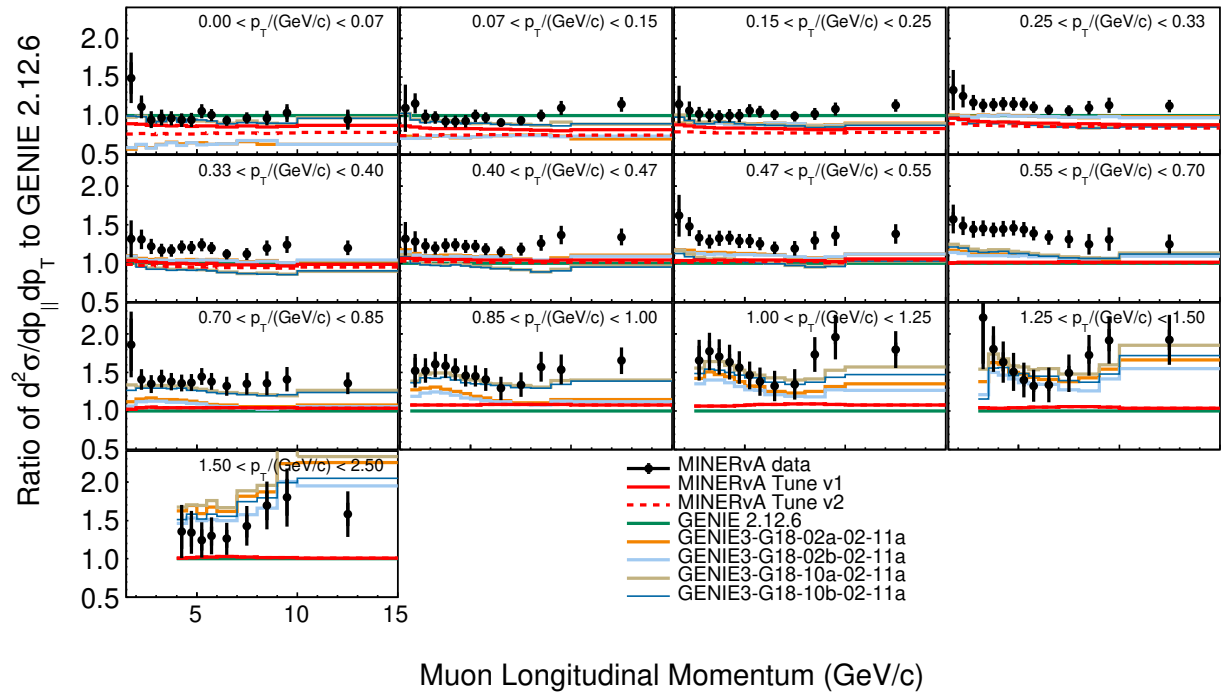


FIG. 10. Ratios of double differential cross sections to GENIE 2.12.6 as a function of muon longitudinal momentum in bins of muon transverse momentum shown for GENIE 2 and tuned models along with GENIE 3 (v3.0.6) models.